Development of a Ground-based Synthetic Aperture Radar System for Highly Repeatable Measurements*

Hoonyol LEE†, Seong-Jun CHO‡, Nak-Hoon SUNG‡ and Jung-Ho KIM‡

†Department of Geophysics, Kangwon National University
Hyoja-dong, Chuncheon, Kangwon-do 200-701, Korea

‡Korea Institute of Geoscience and Mineral Resources
Gajung-dong, Yuseong-gu, Daejeon 305-350, Korea

E-mail: †hoonyol@kangwon.ac.kr, ‡{mac, nhsung, jungho}@kigam.re.kr

Abstract We introduce the development of a robust ground-based synthetic aperture radar (GB-SAR) system capable of obtaining highly accurate SAR images of surface targets repeatedly by dedicated efforts for accurate motion control and innovative system design for stable RF acquisition. A brief introduction of the GB-SAR system and some test images will be followed by the accuracy assessment of the system performance for the future radar-interferometric applications to natural or anthropogenic surface/sub-surface targets.

Key words GB-SAR, synthetic aperture radar, interferometry

1. Introduction

GB-SAR (Ground-Based Synthetic Aperture Radar) is a kind of imaging radar that obtains high resolution 2D image of surface by synthesizing large azimuth aperture from accurate linear motion control of antenna on the ground. As a GB-SAR system can control the motion of the platform very accurately it ensures high repeatability of measurement, which is essential for radar interferometric applications of surface displacement detection such as DInSAR (Differential Interferometric SAR) or PSInSAR (Permanent Scatterer InSAR) techniques.

Contrary to satellite-based SAR systems, a GB-SAR image focusing can reach a theoretically optimal condition due to its zero-Doppler nature, i.e., no instantaneous platform velocity during imaging acquisition, and exact imaging geometry. Thanks to the exact repeatability of the scanning, it provides zero-baseline interferometric configuration for change detection. As maintenance and upgrade of the system is fairly versatile providing arbitrary choices in frequency, polarimetry and incidence angle, it can be also used as a test-bed for a new concept design of airborne or spaceborne SAR system.

There have been indoor GB-SAR experiments in the early 1990s[2][3]. Practical outdoor application of GB-SAR have been performed for the study of building stability [4], landslides [5][6], topography mapping [7][8], agriculture [9][10][11].

In this paper we introduce a GB-SAR system built by one-year's corporative work between Kangwon National University and Korea Institute of Geoscience and Mineral Resources (KIGAM) and present preliminary test images of various polarization and some interferometric applications.

2 . GB-SAR System Configuration

The constructed GB-SAR system is composed of two major parts: the 'RF' part and the 'motion' part (Fig. 1). The RF part is composed of a vector network analyzer (VNA, HP 8753ES), a microwave power amplifier, switch, and two C-band antennas. The

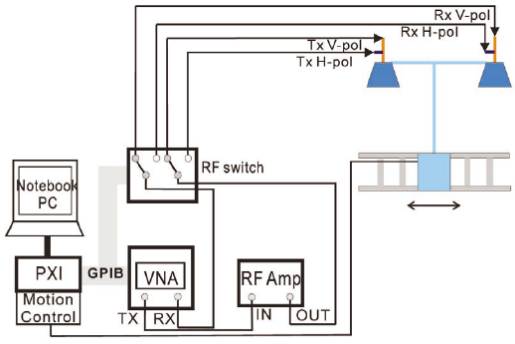

Fig. 1. Configuration of a GB-SAR system.

* This paper is an English-translation of [1] written in Korean.

signal is generated by VNA in a stepped-frequency sweep mode and amplified to 33 dBm before fed into a switch for polarization selection. The signal is then transmitted through the selected port of an antenna. The backscattered signal is fed to the other antenna through a port selected again by switch action for polarization, and recorded by VNA. The two antennas used for transmission and reception separately are identical to each other. They are dual-polarization square horn antenna with orthogonal mode transducer, having bandwidth of 5-5.6 GHz, 20dBi gain, 50dB port isolation, and VSWR of 1.4 (Table 1). By using two antennas for transmission and reception separately and a high power amplifier, we can obtain fully polarimetric SAR images of the target with the distance of several hundreds meters.

The motion part is composed of a 6m rail, two motion controllers, two stepping motors for horizontal and vertical motion. The horizontal motion is for the SAR imaging while the vertical motion capability is also added to the system to obtain a baseline for cross-track interferometric configuration. To prevent signal noise from distortions of cables and connections and to provide the system enough weight for stable operation during the scan, all equipments are onboard the platform that moves along the rail during the scan. Only the power line is attached from outside to the platform.

The accurate estimation of Doppler parameters is essential for the focusing of SAR. As the GB-SAR obtains each line of the image in a stationary state, the Doppler centroid is zero exactly. Also, the value of Doppler rate can be obtained by the exact geometry of the system and the target. GB-SAR is different from other airborne or spaceborne SAR in that the length of synthetic aperture is limited by the physical length of the rail. For a near range case where the synthetic aperture length equal to the antenna beam footprint can be obtained, the azimuth resolution of the GB-SAR image is a half of the real antenna aperture regardless of the range. This is the case of airborne or spaceborne SAR system which we call it here full-focusing is accomplished. For a far range, however, synthetic aperture length is less than the beam footprint of the antenna so that the azimuth resolution of a GB-SAR image is thus a function of range. Different SAR focusing algorithm applies to the above two situations considering the memory usage and computational time. We have developed a GB-SAR focusing processor that employs the range-Doppler algorithm for the full-focusing in near range and the Deramp-FFT algorithm for the partial-focusing in far range.

Table 1. Characteristics of a C-band dual-polarimetric square horn antenna (MTG Inc.).

Item	Characteriscis		Nominal Values	Test Results
Dual-Polarimetric Square Horn Antenna	Frequency (GHz)		5.0~5.6	5.0~5.6
	Beam Width	E-Plane(deg)	15	12.1~13
		H-Plane (deg)	15	15.5~17.5
	Gain (dBi)		20	20.5~21.8
	VSWR		1.5 max.	1.4 max.
	Isolation		35dB	50dB
	Weight (kg)		4 max.	3.1 max.
	Input Impedance (Ω)		50	50

3 . GB-SAR Experiments

A series of GB-SAR experiment was performed to obtain the polarimetric and interferometric images. The system was installed on a roof-top of a 21 m-high building (Fig. 2) looking down the target scene. Fig. 3 depicts the location of the system and an arc-shaped image area overlying an IKONOS satellite image. Table 2 shows the configurations of GB-SAR experiments. Fully polarimetric images (HH, HV, VH, VV) were obtained for each scan. Various images (Table 2) were obtained with different system conditions in time, frequency, and location of antenna to test the potential of the existing SAR and InSAR techniques such as the DInSAR or PSInSAR for surface displacement detection, the Cross-Track InSAR for the generation of Digital Elevation Model (DEM), and Delta-f InSAR by applying frequency shift between two image scans.

Fig. 2. The GB-SAR system and field view of the test site.

Fig. 3. Test site seen from space with a 600m-radius arc image area (Background image: © Google Earth).

Table 2. Configurations for GB-SAR experiments.

Test ID	Date yyyy.mm.dd hh:mm	Purpose	System Configuration
T1	2007.02.16 17:11~17:38	Original	Range: Frequency sweep = 5.2-5.4 GHz, Power = 33 dBm, Sampling number= 1601, IFBW=1 kHz, Full-Polarization. Azimuth: scan length=5 m, step=5 cm.
T2	2007.02.16 17:40~18:06	DInSAR with T1	Same as T1 with temporal baseline of 30 minutes
T3	2007.02.16 18:16~18:41	Cross-Track InSAR with T2	Same as T2 with vertical baseline of -30 cm (30cm down)
T4	2007.02.16 19:26~19:52	Delta-f InSAR with T3	Same as T3 with center frequency shift to 5.29 GHz (frequency baseline of -10MHz)
P1-P9	2007.01.17 15:12~16:48	PSInSAR	Continuous acquisitions with Frequency sweep = 5.15-5.45 GHz, VV only

3.1 Polarimetric SAR images

Fig.4 shows the image obtained in the test T1 with (a) VV, (b) VH, and (c) HH polarization. The range resolution is 0.75m while the azimuth is a function of range: 0.5 m at 100 m range and 3.4 m at 600 m. Trees located at a distance of 100 m are clearly visible in all images. The river banks at 220-270 m range are visible and so is a building at 315-400 m. A system noise that infiltrates the HH polarization image (Fig. 4c) along the central line is due to the coupling effect between the transmission and reception antennas placed horizontally with each other. Fig. 4(d) shows the normalized polarimetric ratio (HH-VV)/(HH+VV) image as a simple example of polarimetric analysis. Trees of high volume scattering show no difference in HH and VV image. Wet grass shows higher value of HH polarization than VV while buildings have higher VV than HH.

3.2 Differential InSAR for target motion detection

GB-SAR provides highly accurate repeatability in the successive measurement of amplitude and phase of the backscattering from targets enabling zero-baseline DInSAR technique for surface displacement detection. Given the two images of a target at R scanned with temporal difference and the target motion r in range direction, the phases ϕ_1 and ϕ_2, the phase difference ϕ, and the rate of phase change with respect to target motion is given as follows:

$$\text{Phases: } \phi_1 = -\frac{4\pi}{\lambda}R_1, \quad \phi_2 = -\frac{4\pi}{\lambda}(R_1 + r) \tag{1}$$

$$\text{Phase diff: } \phi = \phi_2 - \phi_1 = \frac{4\pi}{\lambda}r \text{ (radian)} \tag{2}$$

$$\text{Motion sensitivity: } \frac{\partial\phi}{\partial r} = -\frac{4\pi}{\lambda} \text{ (radian/m)} \tag{3}$$

For C-band (5.3GHz) system the rate of phase change is -12729 deg/m so that 1 mm movement of a target in range direction would cause -12.7° phase change, which is well beyond the phase uncertainty of the system. Fig. 5(a) is an example of DInSAR from two images obtained 30 minutes apart (T2-T1). The phases are unchanged for stable targets such as withered grass, river banks, buildings while the phases are undulating for unstable targets such as forest and shadow regions.

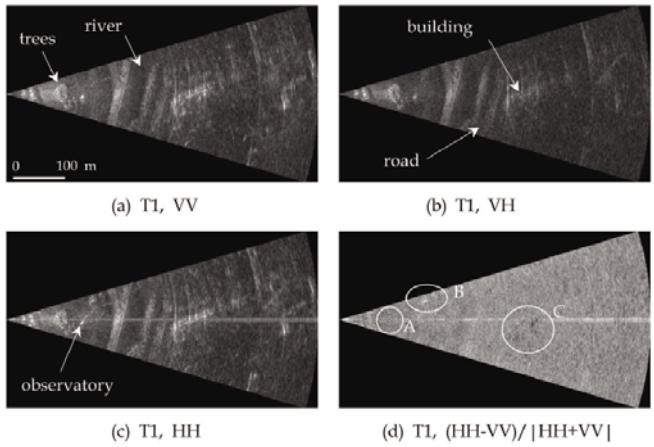

(a) T1, VV (b) T1, VH

(c) T1, HH (d) T1, (HH-VV)/|HH+VV|

Fig. 4. Examples of GB-SAR Polarimetry. (a)-(c) shows the VV, VH, and HH amplitude images of the T1 scene. The normalized difference of polarimetric images (d) shows similar backscattering of HH and VV from the trees (circle A) due to volumetric scattering, higher signal of HH than VV for wet grass (circle B), and lower signal of HH than VV for a building (circle C). The maximum range is 600m.

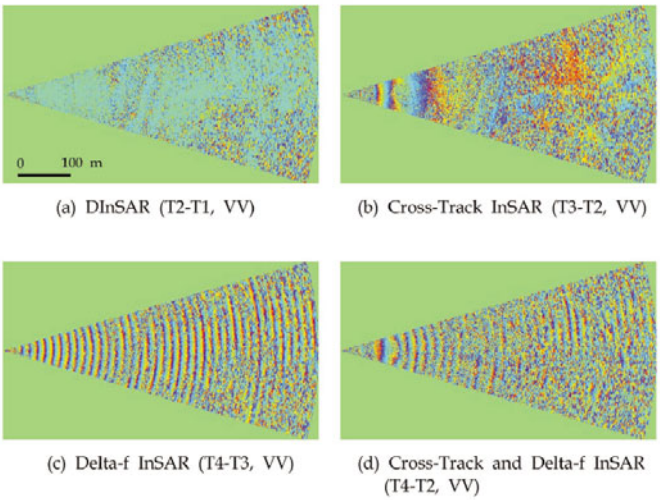

(a) DInSAR (T2-T1, VV) (b) Cross-Track InSAR (T3-T2, VV)

(c) Delta-f InSAR (T4-T3, VV) (d) Cross-Track and Delta-f InSAR (T4-T2, VV)

Fig. 5. Examples of GB-SAR Interferometry. (a) DInSAR with 30-minute temporal baseline. (b) Cross-Track InSAR with -30 cm spatial (vertical) baseline. (c) Delta-f InSAR with -10 MHz frequency baseline. (d) Combination of Cross-Track and Delta-f InSAR. One color cycle (blue to red) indicates the phase change of 360°.

3.3 Cross-Track InSAR for DEM

The phase difference ϕ of two images with a vertical baseline B_v, as shown in Fig. 6, gives an interferometric phase ramp with respect to range and the height sensitivity:

$$\text{Phase: } \phi_1 = -\frac{4\pi}{\lambda}R_1, \quad \phi_2 = -\frac{4\pi}{\lambda}R_2 \tag{4}$$

$$\text{Phase diff.: } \phi \approx -\frac{4\pi}{\lambda}B_v\cos\theta = -\frac{4\pi}{\lambda}B_v\frac{H-h}{R} \ (B_v \ll R) \tag{5}$$

$$\text{Range ramp: } \frac{\partial\phi}{\partial R} \approx \frac{4\pi B_v(H-h)}{\lambda R^2} \tag{6}$$

$$\text{Height sensitivity: } \frac{\partial\phi}{\partial h} = \frac{4\pi B_v}{\lambda R} \tag{7}$$

Fig. 5(b) is the phase difference of T3-T2 with -0.3 m of vertical

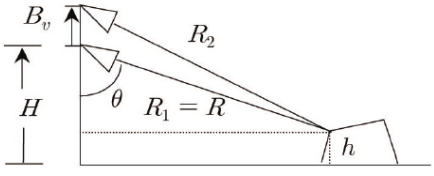

Fig. 6. Cross-Track InSAR configuration.

baseline and H=21 m. The phase ramp is -8.0 deg/m at *R*=100 m and decreases with *R*, which is clearly shown in this figure. The height sensitivity is -38.2 deg/m at *R*=100 m for example. In this experiment, we can confirm that the theoretical interferometric fringes do appear as predicted. Practical usage of the Cross-Track InSAR using the GB-SAR system will be sought after with a dedicated system configuration in the near future.

3.4 Delta-f InSAR

Interferometric phase can be made with a center-frequency difference of $\Delta f = f_2 - f_1$. This is identical to the wavenumber shift of Delta-k InSAR in [12]. The phases, phase difference and phase ramps are as follows.

Phases: $\phi_1 = -\frac{4\pi R}{c} f_1, \quad \phi_1 = -\frac{4\pi R}{c} f_2$ (8)

Phase diff.: $\phi = -\frac{4\pi R}{c}\Delta f$ (9)

Range ramp: $\frac{\partial \phi}{\partial R} = -\frac{4\pi}{c}\Delta f$ (10)

Here c is the speed of light. Fig. 5(c) shows an example of Delta-f InSAR with Δf =-10 MHz. The phase ramp is 24.0 deg/m in this case which shows one-cycle fringe every 15.0 m regardless of the range. The Delta-f InSAR can be used to remove the unwanted phase ramp in the Cross-Track InSAR for DEM generation, which is shown below.

3.5 Cross-Track and Delta-f InSAR

The phases, phase difference, range ramp and height sensitivity of two images with both a vertical baseline (B_v) and a center frequency shift Δf are as follows.

Phases: $\phi_1 = -\frac{4\pi}{c} f_1 R_1, \quad \phi_2 = -\frac{4\pi}{c} f_2 R_2$ (11)

Phase diff.: $\phi \approx -\frac{4\pi}{\lambda}\Delta R - \frac{4\pi R}{c}\Delta f \;\; (\Delta R \ll R, \Delta f \ll f)$

$\approx -\frac{4\pi B_v}{\lambda}\frac{H-h}{R} - \frac{4\pi R}{c}\Delta f \;\; (B_v \ll R)$ (12)

Range ramp: $\frac{\partial \phi}{\partial R} \approx \frac{4\pi B_v (H-h)}{\lambda R^2} - \frac{4\pi}{c}\Delta f$ (13)

Height sensitivity: $\frac{\partial \phi}{\partial h} = \frac{4\pi B_v}{\lambda R}$ (14)

Fig. 5(d) shows the phase difference of T4-T2 within which the principle of Cross-Track and Delta-f InSAR are combined. Here B_v =-0.3 m and Δf =-10 MHz. The range ramp at *R*=100 m, for example, is 16.0 deg/m which is the addition of -8.0 of Cross-Track InSAR and 24.0 of Delta-f InSAR. As the range increases the range ramp effect from Cross-Track InSAR decrease with R^2 and the overall range ramp converges to that of Delta-f InSAR. The height sensitivity is identical to the Cross-Track InSAR case (-38.2 deg/m).

The center frequency of ASAR system onboard the ENVISAT satellite is 5.331 GHz, which is different from ERS-1/2 SAR systems that have 5.3 GHz. With a proper baseline between ENVISAT and ERS-2 satellite orbits, one can have large height sensitivity for Cross-Track InSAR with the reduced range ramp from Delta-f InSAR effect. This technique is called Cross-Interferometry and was recently demonstrated [13]

3.6 PSInSAR for Stable Reflectors

PSInSAR using a GB-SAR system is, in principle, similar to that of spaceborne technique [14] in that it analyzes the interferometric signal from stable scatterers only. However it has many advantages over the spaceborne system due to the highly stable control and repeatability and of GB-SAR system. Firstly the baseline can be controlled accurately and there is no need of guess-work in baseline estimation, Secondly, zero-baseline condition can be obtained so that we do not need extra DEM to remove topographic phase. Third, the path length of microwave is relatively short when compared to airborne or spaceborne SAR system so that the atmospheric path effect is less severe. Lastly, the temporal baseline can be very short, say, tens of minutes, so that relatively rapid surface motion can be monitored with no cyclic phase ambiguity. The data from a local weather station can be used to compensate for the atmospheric effect of GB-SAR interferometry [15], which is very practical when compared to the spaceborne case where there is no way of measuring weather profile along the ray path.

A temporal coherence of *N* complex SAR observations z_i can be defined as

$$\gamma = \frac{\left| \sum_{i=1}^{N} z_i \right|}{\sum_{i=1}^{N} |z_i|} \quad (15)$$

which has the value of $0 < \gamma < 1$. The temporal coherence is a measure of target stability and can be used to select the stable scatterers. The motion accuracy is identical to the case of DInSAR.

Fig. 7 is the temporal coherence of the 9 acquisitions (P1~P9) scanned for approximately two hours (0~400 m only). The temporal coherence is color-coded from zero (black) to one (white) while the value from 0.9 to 1 is redrawn in pseudo-color to highlight the stable scatterers. The phase variation of the stable scatterers (γ >0.9) with time was less than 10˚. For the scatterers with γ >0.99, the phase variation was less than 1˚ which suggests that the 1 mm motion accuracy for stable scatterers can be accomplished with the GB-SAR system.

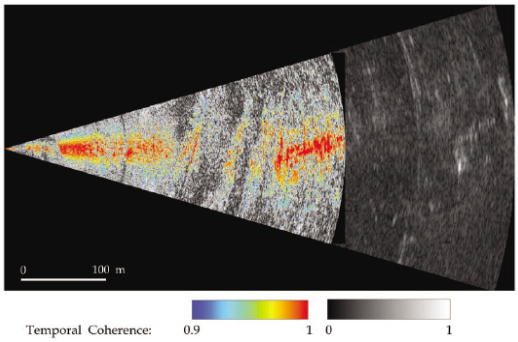

Fig. 7. Temporal coherence of nine acquisitions (P1-P9) for two hours. Coherence value from 0.9 to 1.0 is displayed in color from blue to red, while others in gray scale. Note the stable reflectors such as the withered grass, river banks and buildings maintain the coherence values higher than 0.99 (red). Range greater than 400 m is the SAR amplitude image for comparison.

4. Conclusions

A GB-SAR system capable of highly repeatable measurement was developed and tested for various polarimetric and interferometric applications such as DInSAR, Coherence, Cross-Track InSAR, Delta-f InSAR, and PSInSAR. The system will be applied to the measurement of stability of natural/anthropogenic structures, generation of a high-resolution DEM in local scale, measurement of physical parameters of targets, and even for the concept design for an advanced airborne/spaceborne SAR system.

5. References

[1] Lee, H., S. –J. Cho, N. –H. Sung, and J. –H. Kim, 2007. Development of a GB-SAR (I) : System configuration and interferometry, *Korean Journal of Remote Sensing*, 23(4): 237-245.

[2] Fortuny, J. and A. J. Sieber, 1994. Fast algorithm for a near-field synthetic aperture radar processor, *IEEE Transactions on Antennas and Propagation*, 42(10): 1458-1460.

[3] Nesti, G., J. Fortuny, and A. J. Sieber, 1996. Comparison of backscattered signal statistics as derived from indoor scatterometric and SAR experiments, *IEEE Transactions on Geoscience and Remote Sensing*, 34(5): 1074-1083.

[4] Tarchi, D., H. Rudolf, M. Pieraccini, and C. Atzeni, 2000. Remote monitoring of buildings using a ground-based SAR: application to cultural heritage survey, *International Journc Remote Sensing*, 21(18): 3545-3551.

[5] Leva, D., G. Nico, D. Tarchi, J. Fortuny-Guasch, and A Sieber, 2003. Temporal analysis of a landslide by means ground-based SAR interferometer, *IEEE Transaactions Geoscience and Remote Sensing*, 41(4): 745-757.

[6] Tarchi, D., N. Casagli, R. Fanti, D. D. Leva, G. Luzi, A. Pasuto, M. Pieraccini, and S. Silvano, 2003. Landslide monitoring by using ground-based SAR interferometry: an example of application to the Tessina landslide in Italy, *Engineering Geology*, 68: 15-30.

[7] Nico, G., D. Leva, G. Antonello, and D. Tarchi, 2004. Ground-based SAR interferometry for terrain mapping: Theory and sensitivity analysis, *IEEE Transacations on Geoscience and Remote Sensing*, 42(6): 1344-1350.

[8] Nico, G., D. Leva, J. Fortuny-Guasch, G. Antonello, and D. Tarchi, 2005. Generation of digital terrain models with a Ground-Based SAR system, *IEEE Transactions on Geoscience and Remote Sensing*, 43(1): 45-49.

[9] Brown, S. C. M., S. Quegan, K. Morrison, J. C. Bennett, and G. Cookmartin, 2003. High-resolution measurements of scattering in wheat canopies-implications for crop parameter retrieval, *IEEE Transactions on Geoscience and Remote Sensing*, 41(7): 1602-1610.

[10] Gomez-Dans, J. L., S. Quegan, J. C. Bennett, 2006. Indoor C-band polarimetric interferometry observations of a mature wheat canopy, *IEEE Transactions on Geoscience and Remote Sensing*, 44(4): 768-777.

[11] Zhou, Z. -S., W. -M. Boerner, M. Sato, 2004. Development of a ground-based polarimetric broadband SAR system for noninvasive ground-truth validation in vegetation monitoring, *IEEE Transactions on Geoscience and Remote Sensing*, 42(9): 1803-1810.

[12] Sarabandi, K., 1997. △k-radar equivalent of interferometric SAR's : A theoretical study for determination of vegetation height, *IEEE Transactions on Geoscience and Remote Sensing*, 35(5): 1267-1276.

[13] Adam, N., 2003. First cross interferogram using the radar sensors ENVISAT/ASAR and ERS-2, avaliable online at: http://www.dlr.de/caf/aktuelles/archiv/bilderarchiv/envisat/cross_interferogramm/_cross_interferogramm/cross_interferogramm_en.htm

[14] Ferretti, A., C. Prati, and F. Rocca, 2001. Permanent scatterers in SAR interferometry, *IEEE Transactions on Geoscience and Remote Sensing*, 39(1): 8-20.

[15] Noferini, L., M. Pieraccini, D. Mecatti, G. Luzi, C. Atzeni, A. Tamburini, and M. Broccolato, 2005. Permanent scatterers analysis for atmospheric correction in ground-based SAR interferometry, *IEEE Transactions on Geoscience and Remote Sensing*, 43(7): 1459-1471.